LASER MULTICOMPONENT GAS ANALYSIS OF THE GROUND LAYER OF THE ATMOSPHERE

C.L. Bondarenko, S.I. Dolgii, V.V. Zuev, Yu.S. Kataev, A.A. Mitzel', O.A. Pelymskii, I.V. Ptashnik, K.M. Firsov, and S.F. Shubin

Institute of Atmospheric Optics,
Siberian Branch of the Russian Academy of Sciences, Tomsk
Received March 26, 1992

The results of the theoretical calculation of optimum wavelengths for the detection of the minor gas components in the ground layer of the atmosphere are presented. The experimental results of the investigation of atmospheric gas composition over the industrial zone of Akademgorodok of Tomsk carried out with the laser gas analyzer are obtained as part of the SATOR–91 program. The correlations are found between the temporal variations of concentrations of ozone and carbon dioxide and of ozone and ammonia.

Due to the increasing influence of the human vital activity on the ecology of the environment the problems of the Earth's air protection and, in particular, the problem of monitoring of the variations of the tropospheric and stratospheric ozone concentration, which is the main indicator of the stability of the atmosphere and its resistivity to the penetration of hard ultraviolet radiation into the ground layers and on the Earth's surface have come up most urgently in recent years.

It is well known that although the ozone is a minor component of the atmosphere, its influence on the vital activity processes of nature and humanity is very strong. In the stratosphere, where the significant part of ozone is concentrated, its concentrations may remain unchanged for a long time, while in the troposphere and, particularly, in the ground layer it may undergo strong fluctuations varying in a large range of values depending on the existence and origin of this atmospheric component during days, hours, and sometimes even shorter time intervals.

As is well known, a considerable part of ozone enters the ground layer of the stratosphere owing to the turbulent mixing of the air masses or, sometimes, due to the injections of stratospheric air to the troposphere. The less powerful but quite important natural source of tropospheric ozone is its photochemical formation with the participation of the natural nitrogen oxides and the organic compounds whose existence in the atmosphere is the result of such natural processes as volcano eruptions and forest fires, oxidation–reduction processes with the participation of the microorganisms, photochemical reactions upon exposure to the ultraviolet radiation, processes of soil erosion and the weathering of rocks, etc. However, the ozone concentrations associated with the natural sources usually are not greater than 100 $\mu g/m^3$ (~ 47 ppb) (see Ref. 1).

Recently the photochemical reactions of the nitrogen oxides, sulfur oxides, hydrocarbons, and carbon monoxide of the anthropogenic origin have become the source of the tropospheric ozone (sometimes more powerful than the natural sources). The amount of these components of photochemical reactions rises catastrophically in the ground layer of the atmosphere due to the industrial emission, intensive use of the motor transport, and combustion of liquid and solid fuels at the thermal power stations.

The joint effect of the natural and anthropogenic mechanisms of the ozone production leads to the marked increase of the O_3 concentration not only over the globe but also over territories of individual regions. Although the ozone anthropogenic sources are usually local and observed in highly polluted regions,[1] due to the sufficiently long photochemical lifetime of the ozone–producing components, the high concentrations of O_3 may be transported by air masses along large distances. Thus the extremely high concentrations of ozone were repeatedly recorded in the comparatively pure regions after passage of air masses from the polluted regions at a distance of several hundred kilometres.[2]

In connection with intensification of the pollution of the environment by the industrial waste products, the special attention has been recently paid to the investigation of the negative influence of ozone, nitrogen and sulfur oxides, and organic compounds on the human health, vegetable and animal kingdoms, materials.[3,4,5] For example, according to the data of the USA experts,[6] the effect of high (but not anomalous) concentrations of ozone (more than 240 $\mu g/m^3$) alone substantially decreases productivity of agricultural plants. In addition, ozone, nitrogen, and sulfur oxides are the radiation–sensitive impurities and, therefore, the increase of their concentrations in the atmosphere may influence the radiation balance of Earth and cause significant climate change.[7]

THE PROCESSES OF FORMATION AND DECOMPOSITION OF OZONE IN THE TROPOSPHERE

Let us consider in detail the mechanisms and the chemical reactions of sources and sinks of ozone and other impurity compounds which directly or indirectly affect the variations of the ozone concentration in the atmosphere.

As has been already mentioned above, the photochemical reactions in the stratosphere are the main source of ozone intake to the troposphere (above 20 km) where the molecular oxygen is capable of photodissociating upon exposure to the ultraviolet radiation forming the atomic oxygen in the ground $O(^3P)$ and excited $O(^1D)$ states:

$$O_2 + h\nu(\lambda < 175\ \mu m) \rightarrow O(^1D) + O(^3P)\ , \quad (1)$$

$$O_2 + h\nu(\lambda < 243\ \mu m) \rightarrow O(^3P) + O(^3P)\ . \quad (2)$$

The produced atoms are chemically highly active and in parts of a second recombine with molecular oxygen and the third body M in the upper atmosphere forming ozone

0235-6880/92/06 384-14 $02.00

$$O(^3P) + O_2 + M + O_3 + M \ . \qquad (3)$$

Owing to high reactivity of ozone, its sinks in the atmosphere are caused by a series of the chemical and physical processes (photodissociation in the upper atmosphere, reactions with the atomic oxygen and hydrogen and with the hydrogen radicals and nitrogen components of the atmosphere). Without giving the chemical reaction equations, which are elaborately considered in Refs. 8 and 9, let us recall that the process of methane (CH_4) oxidation in air (by intermediate reactions of such carbon components as methoxyl CH_3O, formaldehyde CH_2O, hydroperoxide HO_2, with molecular oxygen and oxide NO and dioxide NO_2 of nitrogen) is considered to be one more natural source of ozone intake to the troposphere.

The active nitrogen compounds: NO, NO_2, NO_3, N_2O_5, $ClONO_3$, HNO_3, and HNO_4 forming series of the so–called odd nitrogen NO_x (see Ref. 8) always exist in the atmosphere. Among them the nitrogen oxide NO and dioxide NO_2 make the most important contribution to the formation and decomposition of tropospheric ozone. The exhausts of high–temperature products of combustion of fuel of different kind (motor transport, industry, and thermal power stations) are the anthropogenic sources of their entering into the atmosphere. The microbiological processes in the soil and the photochemical oxidation of ammonia and nitrogen dioxide in the atmosphere[10] are related to the natural sources. Omitting the chemical reactions of NO and NO_2 formation (which were considered in detail in Ref. 10), we give the reactions directly affecting the variations of the ozone concentration solely.

Upon exposure to the UV radiation the nitrogen dioxide is capable to photodissociate producing atomic oxygen

$$NO_2 + h\nu(\lambda < 400\ \mu m) \rightarrow NO + O \ , \qquad (4)$$

which through a three–body reaction produces ozone (see Eq. (3)). However, the ability of NO_2 and NO to react with O_3 yields the powerful mechanism of the ozone sink

$$NO_2 + O_3 \rightarrow NO_3 + O_2 \ ; \qquad (5)$$

$$NO + O_3 \rightarrow NO_2 + O_2 \ . \qquad (6)$$

Thus, the nitrogen dioxide can participate in both sink and generation of tropospheric ozone.

Sulfur dioxide[10] and water vapor[8] affect very strong the variation of the ozone concentration. Figure 1 shows the diagram generalizing the interaction mechanisms and the photochemical reactions in which the minor gas components of the atmosphere (containing hidrogen, carbon, and nitrogen) contribute to the formation and sink of tropospheric ozone.

Thus, the variations of the ozone concentration in the ground layer may be accompanied by the variation in the concentrations of trace components of the atmosphere, such as oxides of nitrogen and sulfur, hydrocarbons, freons, etc., entering the ozone cycle. Therefore, by monitoring in a proper way the variation of the concentration of the gaseous trace components of the ground layer and taking into account the temperature and wind stratification of the Earth's atmosphere, we can predict the anthropogenic and natural variations of the ozone concentration. From the viewpoint of detection of the concentrations of substances of from 0.01 to 10 ppm for molecules and from 0.01 to 10 ppb for metal vapors, the method of direct chemical sampling is most accurate. It is a highly sensitive method but most often has insufficiently fast response. For routine remote monitoring of the environment, the methods of laser gas analysis are most suitable. These methods satisfy the standards of highly concentration sensitivity and selectivity and have fast response[11,15] for detection of minor gas impurities under conditions of fast–varying processes in the ground layers of the atmosphere. In spite of the variety of laser gas–analysis methods, the method of differential absorption in the near– and middle infrared ranges is the simplest one from the viewpoint of technical realization, first, because of the high level of informational content of these ranges due to the fact that the absorption lines of the most part of minor gas impurities of the atmosphere lie in these ranges and, second, due to the availability of high–power tunable lasers and the frequency parametric converters whose spectral bands cover the absorption lines of the gases participating in the ozone cycle.

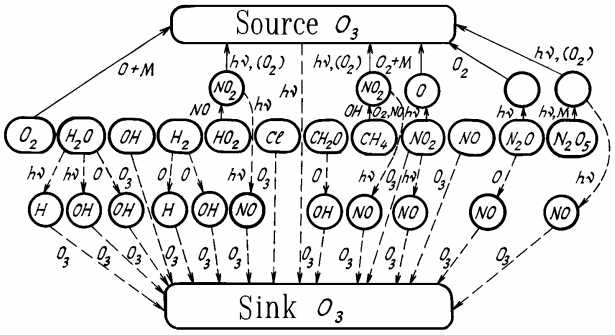

FIG. 1. Diagram showing the interaction of the minor gaseous components in the troposphere.

THE METHOD OF OPTIMUM WAVELENGTH SELECTION

The relationship of the measurable signal with the concentration ρ of the *i*th gas in the base gas analyzer is given by the well–known equation

$$P(\lambda) = P_0(\lambda)\,\eta(\lambda)\exp[-\rho_i k_i(\lambda)L - \beta_i(\lambda)] \ , \qquad (7)$$

where $P_0(\lambda)$ and $P(\lambda)$ are the mean radiation power at the input and output from the atmospheric channel at the wavelength λ, η(λ) is the instrumental function of the measuring system including the efficiency of the photodetector and the receiving–transmitting optics, the degree of the beam interception, the reflectance of a target, and other losses, $k_i(\lambda)$ is the absorption coefficient of the examined *i*th gas at the wavelength λ (the method of its calculation is described below), L is the length of the path, ρ_i is the examined gas concentration averaged over the path; $\beta_i(\lambda)$ is the background optical thickness, i.e., the optical thickness of all interfering gases except the *i*th one, aerosol and water continuum components of attenuation

$$\beta_i(\lambda) = \sum_{j \neq i} L\rho_j^{bg} k_j(\lambda) + \beta_a(\lambda) + \beta_c(\lambda) \ . \qquad (8)$$

where ρ_j^{bg} is the background concentration of the *j*th gas, $\beta_a(\lambda)$ is the aerosol optical thickness, and $\beta_c(\lambda)$ is the water continuum optical thickness.

When using the two–wave measuring method (the method of differential absorption) the concentration of the ith gas is determined from the comparison of signals at two wavelengths lying on (λ_{on}) and off (λ_{off}) the absorption line

$$\rho_i = \frac{1}{L\Delta k_i}\left[\ln\frac{P(\lambda_{off})}{P(\lambda_{on})} + \Lambda_i\right]; \quad (9)$$

$$\Lambda_i = \ln\frac{P_0(\lambda_{on})\,\eta_{on}}{P_0(\lambda_{off})\,\eta_{off}} - \Delta\beta_i; \quad (10)$$

$$\Delta\beta_i = \beta_i(\lambda_{on}) - \beta_i(\lambda_{off}) = \sum_{j\neq i} L\rho_j^{bg}\Delta k_j + \Delta\beta_a + \Delta\beta_c, \quad (11)$$

where $\Delta\beta_i$ is the differential background for the examined ith gas,

$$\Delta k_i = k_i(\lambda_{on}) - k_i(\lambda_{off}); \quad \Delta\beta_a = \beta_a(\lambda_{on}) - \beta_a(\lambda_{off});$$
$$\Delta\beta_c = \beta_c(\lambda_{on}) - \beta_c(\lambda_{off}).$$

In this paper the optimum wavelengths are selected for the base gas analyzer based on the CO and CO_2 lasers, operating at the fundamental and transformed frequencies. The informative wavelengths are selected for the one–wave and two–wave measurement methods.

The method for selecting the wavelength pairs in order to achieve the maximum concentration sensitivity of the two–wave laser gas analyzer was proposed in Ref. 20. The basic physical principles of this method qualitatively correctly describe the measurement conditions under which the maximum sensitivity is achieved.

In this paper we use the statistic criterion for the selection of the optimum wavelength, which allows us to take into account not only the fundamental physical trends in the behavior of the laser radiation energy absorption by the molecules of examined and interfering gases at different wavelengths but also the statistical information about the content of the gases, aerosol extinction, as well as the statistics of the measurable signals.

Let us briefly consider the mathematical algorithm for selection of the optimum wavelengths used in the differential absorption method. Assuming η to be independent of λ and t lying within the given spectral and temporal measurement intervals (i.e., $\eta_{off} = \eta_{on}$), we rewrite Eq. (9) in the following form:

$$\rho = \frac{1}{L\Delta k}(y - \Delta\beta), \quad (12)$$

where $y = \ln\left[\frac{P(\lambda_{off})P_0(\lambda_{on})}{P(\lambda_{on})P_0(\lambda_{off})}\right]$ is a certain generalized measurement result depending on the measurable quantities: $P(\lambda_{off})$, $P(\lambda_{on})$, $P_0(\lambda_{off})$, and $P_0(\lambda_{on})$.

We will assume in Eq. (6) the quantities $\Delta\beta$ and ρ together with the measurable quantity y to be random. These circumstances determine the statistical approach to the solution of the problem of the selection of the informative wavelength. Mathematically the problem of optimum wavelength selection may be considered as that of the gas object identification from the signals being measured. To solve this problem, we use the Bayes criterion of detection which minimizes the mean risk.[21] The general algorithm was described in Ref. 22 where the criterion for the informative spectral–section determination was proposed for solving the gas analysis problem with the help of the OAD.

In general the criterion has a form

$$R(\lambda) \underset{\lambda}{\rightarrow} \min, \text{ or } R(\lambda) \le R_0, \quad (13)$$

where $R(\lambda)$ is the mean risk at the wavelength λ and R_0 is the threshold value of the mean risk. The mean risk is given by the well–known formula (see, for example, Ref. 21)

$$R(\lambda) = q\Pi_{11} + p\Pi_{21} + q(\Pi_{12} - \Pi_{11})\varepsilon_1(\lambda) - p(\Pi_{21} - \Pi_{22})(1 - \varepsilon_2(\lambda)), \quad (14)$$

where Π_{ij} are the elements of the matrix of losses, q and $1 - q = P$ are the *a priory* probabilities of the fact that the unknown parameter ρ belongs to the nonintersecting classes of states X_1 and X_2, ε_1 and ε_2 are the probabilities of errors of the first– and second kinds.

To calculate ε_1 and ε_2, we must have the probability density functions $P(y\,|\,\rho \in X_n)$; $\omega_n(\rho)$ for $n = 1, 2$; and, $\varphi(\Delta\beta)$ and the boundaries of the regions Y_1 and Y_2.[20,21]

Let us consider the form of the probability distribution of the parameters y, ρ, and $\Delta\beta$ entering into Eq. (12).

1) We will assume the conditional distributions in both hypotheses $P(y\,|\,\rho \in X_n)$ to be normal with the parameters $(\bar{y}_n, \sigma^2_{y_n})$ where $\bar{y}_n$ and $\sigma^2_{y_n}$ are the mean value and the variance of y for the hypotheses $n = 1$ ($\rho = 0$) and $n = 2$ ($\rho \neq 0$),

$$\bar{y}_1 = \Delta\beta; \quad \bar{y}_2 = \rho L\Delta k + \Delta\beta. \quad (15)$$

The variance σ_{yn} depends on the error in measuring the received signal. According to Refs. 22 and 23 for recording and digital processing systems conventionally used in experiments, the acceptable value of logarithm of the ratio of the signals received at the wavelengths λ_{on} and λ_{off} must satisfy the condition $\ln[\tilde{P}(\lambda_{off})/\tilde{P}(\lambda_{on})] \ge 0.01$. Starting from this, let us assume that $\sigma_{y_1} = \sigma_{y_2} = \sigma_y = 0.01$. $\tilde{P}(\lambda_{off}) = P(\lambda_{off})/P_0(\lambda_{off})$; $\tilde{P}(\lambda_{on}) = P(\lambda_{on})/P_0(\lambda_{on})$.

2) We will approximate the *a priory* distribution $\omega_2(\rho)$ by the normal distribution with the parameters ρ and σ^2_ρ, where $\sigma^2_\rho = \sigma_{fl}\bar{\rho}$ and δ_{fl} is determined primarily by the unaveraged turbulent air fluctuations on the beam path in the period between the measurements at the wavelengths λ_{off} and λ_{on} with δ_{fl} taken to be equal to 0.01–0.05. The probability density function is assumed to be the δ–function: $\omega_1(\rho) = \delta(\rho - \bar{\rho}_1)$ with the parameter $\bar{\rho}_1 = 0$.

3) We will assume the distribution $\varphi(\Delta\beta)$ to be the normal one with the same parameters $(\Delta\bar{\beta}, \sigma_{\Delta\beta})$ for both hypotheses (n = 1, 2), where the mean differential background $\Delta\bar{\beta}$ is given by Eq. (11).

When the variance $\sigma_{\Delta\beta}$ was assigned, two factors were taken into account.

a) The fluctuations $\beta(\lambda, t)$ are caused by the air turbulent fluctuations and contribute $\simeq \delta_{fl}(\beta^2_{on} + \beta^2_{off})^{1/2}$ (in the approximation $\sigma_\beta \simeq \delta_{fl}\beta$) to the variance $\sigma_{\Delta\beta}$. The background level both on line and off line, i.e., β_{on} and β_{off} was calculated from Eq. (8).

b) The systematic error of the $\Delta\beta$ determination is caused by the deviation of the *a priory* assigned values of β_a and β_c in Eq. (11) and the background concentrations of interfering gases from their real values during the measurements. This error makes the contribution $\approx \delta_{sys}|\Delta\overline{\beta}|$ to $\sigma_{\Delta\beta}$. The value of δ_{sys} was assigned in the range 0.01 – 0.30 (see Ref. 25).

The following approximate equation for the variance $\Delta\beta$ has been obtained with an account of the above–given factors:

$$\sigma_{\Delta\beta} = \delta_{fl}(\delta_{sys} + 1.0)(\beta_{off}^2 + \beta_{on}^{2\ 1/2} + \delta_{sys}|\Delta\overline{\beta}| \qquad (16)$$

(the factor $(\delta_{sys} + 1.0)$ arises due to the correlations between the two above–indicated factors). Formula (16) allows us to take into account more accurately the effect of the background on the mean risk and, hence, on the minimum detectable concentration for the given pair of wavelengths.

Using the above–determined distributions $P(y|\rho\in X_n)$, $\omega_n(\rho)$, and $\varphi(\Delta\beta)$ we obtain the following equations for ε_1 and ε_2:

$$\varepsilon_1 = \frac{1}{2}[2 - \Phi(g_{11}) - \Phi(g_{12})]\ ; \qquad (17)$$

$$\varepsilon_2 = \frac{1}{2}[\Phi(g_{21}) - \Phi(g_{22})]\ ,$$

where $\Phi(g)$ is the error function $\Phi(g) = \frac{2}{\sqrt{\pi}}\int_0^g e^{-t^2}dt$.

$$g_{nm} = \left|\frac{u_n - M_m}{\sqrt{2}\sigma_m}\right|\ ;\ n = 1, 2\ ;\ m = 1, 2\ .$$

$$M_1 = \Delta\overline{\beta}\ ,\ M_2 = \overline{\rho}L\Delta k + \Delta\overline{\beta}\ , \qquad (18)$$

$$\sigma_1 = \sqrt{\sigma_y^2 + \sigma_{\Delta\beta}^2}\ ,\ \sigma_2 = \sqrt{\sigma_y^2 + \sigma_{\Delta\beta}^2 + L^2\Delta k^2\sigma_\rho^2}\ ,$$

$\sigma_y = 0.01$, $\sigma_\rho = (0.01 - 0.05)\overline{\rho}$, and u_1 and u_2 are the boundaries of intersection of the intervals Y_1 and Y_2 which are determined by means of solving the equations

$$q\frac{(\Pi_{12} - \Pi_{11})}{\sigma_1}\exp\left[-\frac{1}{2\sigma_1^2}(y - M_1)^2\right] =$$

$$= p\frac{(\Pi_{21} - \Pi_{22})}{\sigma_2}\exp\left[-\frac{1}{2\sigma_2^2}(y - M_2)^2\right]. \qquad (19)$$

It should be noted that Eqs. (17) and (18) are valid when the condition $\overline{\rho}/\sigma_\rho > 3$ is satisfied.

The equations allow us to determine the most informative spectral sections for solving the detection problem when examining two hypotheses: H_2 is with gas in the mixture and H_1 is without gas in the mixture. The minimum detectable gas concentration (for the given pair of wavelengths λ_{on} and λ_{off}) was determined given that

$$R_0(\lambda_{off}, \lambda_{on}) = 10\ \%\ .$$

For the one–wave method, Eqs. (9), (12), (15), (16), and (18) are reduced to the form:

$$\rho = 1/kL(y - \beta(\lambda))\ ;\ \overline{y}_1 = \beta\ ;\ \overline{y}_2 = \beta + \rho\kappa L\ ;$$

$$y = \ln[P(\lambda)/P_0(\lambda)]\ ;\ M_1 = \overline{\beta}\ ;\ M_2 = \overline{\beta} + \overline{\rho}kL\ ;$$

$$\sigma_1 = \sqrt{\sigma_y^2 + \sigma_\beta^2}\ ,\qquad \sigma_2 = \sqrt{\sigma_y^2 + \sigma_\beta^2 + L^2k^2\sigma_\rho^2}\ ; \qquad (20)$$

$$\sigma_\beta = \delta_{fl}(\delta_{sys} + 1.0)\ \overline{\beta} + \delta_{sys}\ \overline{\beta}\ ,$$

where the mean background β is determined from Eq. (8).

In the case of the one–wave method the quantities β_a and β_c will make (in comparison with the differential absorption) much larger contribution to δ_β.

The risk calculations were made for the following values of the elements of the matrix losses: $\Pi_{12} = \Pi_{21} = 1$ and $\Pi_{22} = \Pi_{11} = 0$. The *a priory* probabilities were taken to be equal $q = p = 0.5$. The calculation was made for 2–km path.

It should be noted that in Refs. 20 and 21 the maximum interval between λ_{off} and λ_{on} did not exceed 5 cm^{-1} and therefore the effect of aerosol and water continuum, which leads to the significant errors for the intervals longer than 5 cm^{-1}, was ignored. In this paper an account of the aerosol and water continuum makes it possible to extend this interval up to $\simeq 30$ cm^{-1} (further extension is undesirable because of marked increase of time required for laser tuning).

ABSORPTION COEFFICIENT MODELING

To deal with the gas analysis problems, it is necessary to have the information about the absorption coefficients of the atmospheric air and the sounded gases. The state–of–the–art of investigations enables us to calculate the molecular absorption coefficients for real atmospheric conditions. The information about the background concentrations of atmospheric gas components,[28,29] atlases of the line parameters,[16,17] and the line profiles near the line center and for large resonant frequency detunings[31] are currently available.

In calculations of the molecular absorption coefficients on the near–ground paths in the IR, we can use, the Lorentzian line shape[30] k_ν($cm^{-1}\cdot atm^{-1}$) which has the form

$$k_\nu = \sum_i \frac{S_i}{\pi}\frac{\gamma_i}{(\nu - \nu_i)2 + \gamma_i^2}\ , \qquad (21)$$

where ν_i, S_i, and γ_i are the position of the center, strength, and half-width of the ith line, respectively. In our calculations of absorption coefficients the contributions of the spectral lines from the spectral interval $[\nu - \Delta\nu, \nu + \Delta\nu]$ (where $\Delta\nu = 5$ cm^{-1}) are taken into account.

The calculations of absorption coefficients were performed based on the atlas published in Ref. 16 for 90 frequencies of the CO_2 laser, for 66 frequencies of the CO laser, and for 3055 summed frequencies of the CO laser and second harmonic of the CO_2 laser. The absorption coefficients were calculated at each frequency for all the 28 gases whose parameters were given in the HITRAN atlas.[16]

To determine the optimal wavelength for sounding of atmospheric gas components, it is necessary to compare the volume molecular absorption coefficient of air (km^{-1})

$$\alpha_\nu = \sum_{m\neq n} k_\nu^{(m)}\rho_m\ , \qquad (22)$$

with that of the nth gas $\alpha_\nu^{(n)}$. The background gas concentrations ρ_m are taken from Ref. 28. The use of the *a priory* calculated profiles $k_\nu^{(m)}$ allows us to change in real

time and in a wide range the background concentration of the mth gas component and to determine the limiting detectable values ρ_n. The calculated absorption coefficients of the air and the examined gas are plotted. The absorption spectrum fragments for the summed frequencies of the CO_2 and CO lasers are shown in Fig. 2*a*. The solid curves denote the air absorption coefficients, the vertical lines – the absorption coefficients of the examined gases. The absorption spectra for the second and fundamental harmonics of the CO_2 laser are shown in Figs. 2*b* and *c*. It can be seen from these figures which transitions are the most informative ones for recording the above–listed gases.

THE RESULTS OF THE OPTIMUM WAVELENGTH SELECTION

The calculations were made for 10 examined gases with an account of all the 28 gases, whose parameters were given in the HITRAN atlas.[16] The results of modeling by the differential absorption method for $L = 2$ km, $R_0 = 10\%$, and $\sigma_y = 0.01$ are presented in Table I.

The examined gases together with their background concentrations, the obtained wavelength pairs (the wavelength corresponding λ_{on} are indicated above), the differential absorption coefficients (DAC) Δk, and the differential background (DBG) $\Delta\beta$ evaluated from Eq. (5) are given in the columns 1–4. The calculation of $\Delta\beta$ was performed with an account of the aerosol component following the Krekov–Rakhimov model[26] and the continuum absorption of H_2O (in the region 8–12 km) according to the Aref'ev[27] empirical formula. The minimum detectable concentrations (MDC) for small ($\delta_{sys} = 0.01$) and large ($\delta_{sys} = 0.3$) systematic errors are presented in columns 5 and 6. The smaller value of the MDC corresponds to $\delta_{fl} = 0.01$, and the larger one – to $\delta_{fl} = 0.05$. The results of the MDC calculation borrowed from Ref. 20 are given in column 7. The MDC calculated in this paper, on the average, is twice as large as the MDC obtained in Ref. 6, which is mainly explained by the fact that in our paper the complete statistical account of such factors affecting the MDC as: the background level (or the differential background level $\Delta\beta$ in the differential method) which included the aerosol and continuum components of absorption, the related error σ_β ($\sigma_{\Delta\beta}$); the error of signal measuring σ_y; and, the error due to the turbulent air fluctuations on the path σ_ρ. Moreover, all the calculations were made for the given error probability (the risk R_0) of MDC recording. At the same time only the qualitative evaluation of the MDC was given in Ref. 20, as a consequence, the obtained values of the minimum detectable concentration were somewhat underestimated.

The results presented in Table I allow us to select the pairs most stable in the sense of the systematic error δ_{sys} (arising due to the deviation of the *a priory* assigned background level β from its real value during the measurement (see above)). For example, it can be seen that the pair $2 \times 9P(36)$ and $2 \times 9P(30)$ is the most stable one in the sense of the systematic error: the increase of δ_{sys} from 0.01 to 0.30 leads to the increase of the MDC only by a factor of two, at the same time for the rest of 4 pairs the MDC increases by a factor of 4–10. Obviously, this is related to the significant contribution of $\delta_{sys}|\Delta\overline{\beta}|$ (see Eq. (18)) for these pairs as a consequence of a larger (than for the other pairs) value of $\Delta\overline{\beta}$. The weak MDC dependence on the systematic error in the differential method takes place also for the following gases: CH_4, C_2H_4, NO_2, H_2O, and O_3 for all the selected wavelength pairs; NH_3 for all the pairs except [$9R(38)$ and $9R(24)$], CO for the wavelength pairs $2 \times [9R(30)$ and $9R(28)]$, $2 \times [9R(30)$ and $9R(26)]$, and $2 \times [9R(30)$ and $9R(34)]$, i.e., actually for all the examined gases for the most part of the selected pairs.

For such gases as NO_2 and CH_4 and for several wavelength pairs of CO, the weak MDC dependence on the random error δ_{fl} (see above) is also observed. The increase of δ_{fl} from 0.01 to 0.05 leads to the growth of the MDC of these gases by 30–50%, while for the other gases the MDC increases by a factor of 3 and more. This relatively weak dependence on δ_{fl} is obviously explained by the lower (than for the other pairs) total background level $\sqrt{\beta_{off}^2 + \beta_{on}^2}$ (see Eq. (16)).

Somewhat different situation is observed for the base one–wave gas analyzer, as can be seen from Table II (see Eq. (20)). The calculations were made for the same conditions: $L = 2$ km, $R_0 = 10\%$, $\delta_y = 0.01$; and for the same levels of background concentrations ρ_j^{bg} of the gases as in the differential method). The obtained MDC for the small systematic error $\delta_{sys} = 0.01$ practically does not differ from the MDC calculated by the differential absorption method, but at the same time for $\delta_{sys} = 0.3$ the minimum detectable concentrations with the use of the one–wave method on the average, by a factor of 12–15. The smaller amount of the MDC increase is observed only for NO_2, CH_4, and CO at $2 \times 9R(30)$. It may also be explained by means of Eq. (18) because in the differential method the main contribution to the systematic error $\sigma_{\Delta\beta}$ comes from the factor $|\Delta\overline{\beta}|$ which usually is small in comparison with the mean background $\sqrt{\beta_{off}^2 + \beta_{on}^2}$ which in general represents the contribution of the random error to $\delta_{\Delta\beta}$; in the one–wave method the contribution of the systematic error to δ_β is proportional to $\overline{\beta}$ (see Eq. (22)) and therefore its influence on the value of δ_β and, consequently, on the MDC is more significant.

Thus, the results of the MDC modeling for the one–wave method also allow us to indicate the most effective wavelengths for the quantitative analysis of multicomponent gaseous mixtures under conditions of overlapping of the absorption bands (lines) of examined and interfering gases. However, the sufficiently accurate determination of the gas concentrations can be obtained in this case only from the inverse problem solution based on the data of multiwave sounding.

TABLE I. Results of selection of the optimum line pairs for measuring with the help of the base gas analyzer by the differential absorption technique for $L = 2$ km, $\sigma_y = 0.01$, *and* $R_0 = 10\%$.

Gas, ρ_{bg} (ppm)	Line pairs	DAC (cm^{-1} atm^{-1})	DBG ($\Delta\beta$)	MDC (ppm) $\delta_{fl} = 0.01–0.05$		Ref. 5
				$\delta_{sys} = 0.01$	$\delta_{sys} = 0.03$	
H_2O ($1.9 \cdot 10^4$)	10*P*(40) 10*P*(38)	$1.5 \cdot 10^{-3}$	−0.012	120–400	180–550	
	10*P*(40) 10*P*(34)		−0.026			
	10*P*(40) 10*P*(32)		−0.032			
	10*P*(40) 10*P*(30)		−0.032			
	10*R*(20) 10*R*(18)	$6.6 \cdot 10^{-4}$	−0.005	280–970	340–1250	165
CO_2 (330)	2× 9*P*(36) 9*P*(30)	0.009	0.036	25–90	44–148	
	2× 9*P*(36) 9*P*(38)		0.58		270–350	
	2× 9*P*(36) 9*P*(32)		0.86		390–470	
	2× 9*P*(36) 9*P*(26)		0.68		320–400	
	2× 9*P*(36) 9*P*(24)		−0.18		110–220	
	8–7*P*(20) 9–8*P*(20)	0.7	−0.56	0.41–1.60	3.1–5.0	
NO ($3 \cdot 10^{-4}$)	2× 10*P*(24) 10*P*(26)	2.5	0.40	0.11–0.44	0.73–1.16	0.041
	2× 10*P*(24) 10*P*(14)		−0.38	0.14–0.60	0.73–1.33	
O_3 (0.03)	9*P*(14) 9*P*(24)	11.3	0.022	0.015–0.06	0.019–0.08	0.005
	9*P*(14) 9*P*(22)	10.3	0.008			
	9*P*(12) 9*P*(24)	11.0	0.0026			
	9*P*(12) 9*P*(22)	10.0	−0.012			
NH_3 ($5 \cdot 10^{-4}$)	9*R*(30) 9*R*(28)	78	−0.011	0.002–0.007	0.003–0.009	0.001
	9*R*(30) 9*R*(26)		−0.34		0.004–0.010	
	9*R*(30) 9*R*(34)		0.05		0.004–0.010	
	9*R*(30) 9*R*(32)		−0.014		0.003–0.009	
	10–9*P*(15)+9*R*(16) 10–9*P*(15)+9*R*(14)					
CH_4 (1.7)	10–9*P*(17)+9*R*(30) 10–9*P*(19)+9*R*(22)	3.7	0.0003	0.03–0.045	0.04–0.055	
	10–9*P*(17)+9*R*(30) 10–9*P*(21)+9*R*(10)		0.0024			
	10–9*P*(17)+9*R*(30) 10–9*P*(22)+9*R*(34)		0.0032			
	11–10*P*(18)+9*R*(28) 11–10*P*(21)+9*P*(6)		0.0011			

TABLE I. (continued).

Gas, ρ_{bg} (ppm)	Line pairs	DAC (cm^{-1} atm^{-1})	DBG ($\Delta\beta$)	MDC (ppm) d_{fl} = 0.01–0.05		Ref. 5
				δ_{sys} = 0.01	δ_{sys} = 0.03	
CH_4 (1.7)	11–10*P*(18)+9*R*(28) 12–11*P*(19)+9*R*(32)	3.1	0.0024	0.045–0.06	0.05–0.065	
	11–10*P*(18)+9*R*(28) 10–9*P*(21)+9*R*(10)		−0.001			
	11–10*P*(18)+9*R*(28) 11–10*P*(21)+9*R*(24)		0.0028			
NO_2 ($2.3\cdot10^{-5}$)	10–9*P*(19)+9*R*(34) 10–9*P*(19)+9*R*(8)	3.5	0.042	0.04–0.06	0.055–0.09	
	10–9*P*(19)+9*R*(34) 10–9*P*(19)+9*R*(14)	3.4	0.003			
	10–9*P*(19)+9*R*(34) 10–9*P*(19)+9*R*(12)	3.5	0.007			
	10–9*P*(19)+9*R*(34) 10–9*P*(22)+9*R*(32)		0.013			
	10–9*P*(19)+9*R*(34) 10–9*P*(21)+9*R*(22)	3.6	−0.09			
	10–9*P*(19)+9*R*(20) 11–10*P*(19)+9*R*(24)	3.2	−0.01			
	10–9*P*(19)+9*R*(20) 11–10*P*(20)+9*R*(26)	3.0	−0.005			
C_2H_4 (0.02)	10*P*(14) 10*P*(12)	29	0.022	0.005–0.020	0.008–0.03	0.002
	10*P*(14) 10*P*(28)	34	0.032			
	10*P*(14) 10*P*(22)	33	0.007			
	10*P*(14) 10*P*(30)		0.044			
	10*P*(14) 10*P*(8)		0.048			
	10*P*(14) 10*P*(20)		−0.015			
	10*P*(14) 10*P*(18)	31	−0.006			
C_6H_6 (0.005)	9*P*(30) 9*P*(24)	1.3	0.036	0.09–0.036	0.20–0.62	0.031
	9*P*(30) 9*P*(36)		−0.03			
	9*P*(30) 9*P*(26)		−0.022			
CO (0.15)	2× 9*R*(30) 9*R*(28)	24	−0.012	0.006–0.008	0.007–0.012	
	2× 9*R*(30) 9*R*(26)		−0.024			
	2× 9*R*(30) 9*R*(34)		−0.022			
	2× 9*R*(30) 9*R*(32)	23	−0.24	0.006–0.013	0.042–0.053	
	2× 9*P*(24) 9*P*(26)	23.0	0.14	0.007–0.019	0.030–0.048	0.004

Note: Negative value of $\Delta\beta$ means that $\beta(\lambda_{on}) < \beta(\lambda_{off})$, see Ref. 5 (upon substituting into Eq. (4) the sign of $\Delta\beta$ must be taken into account).

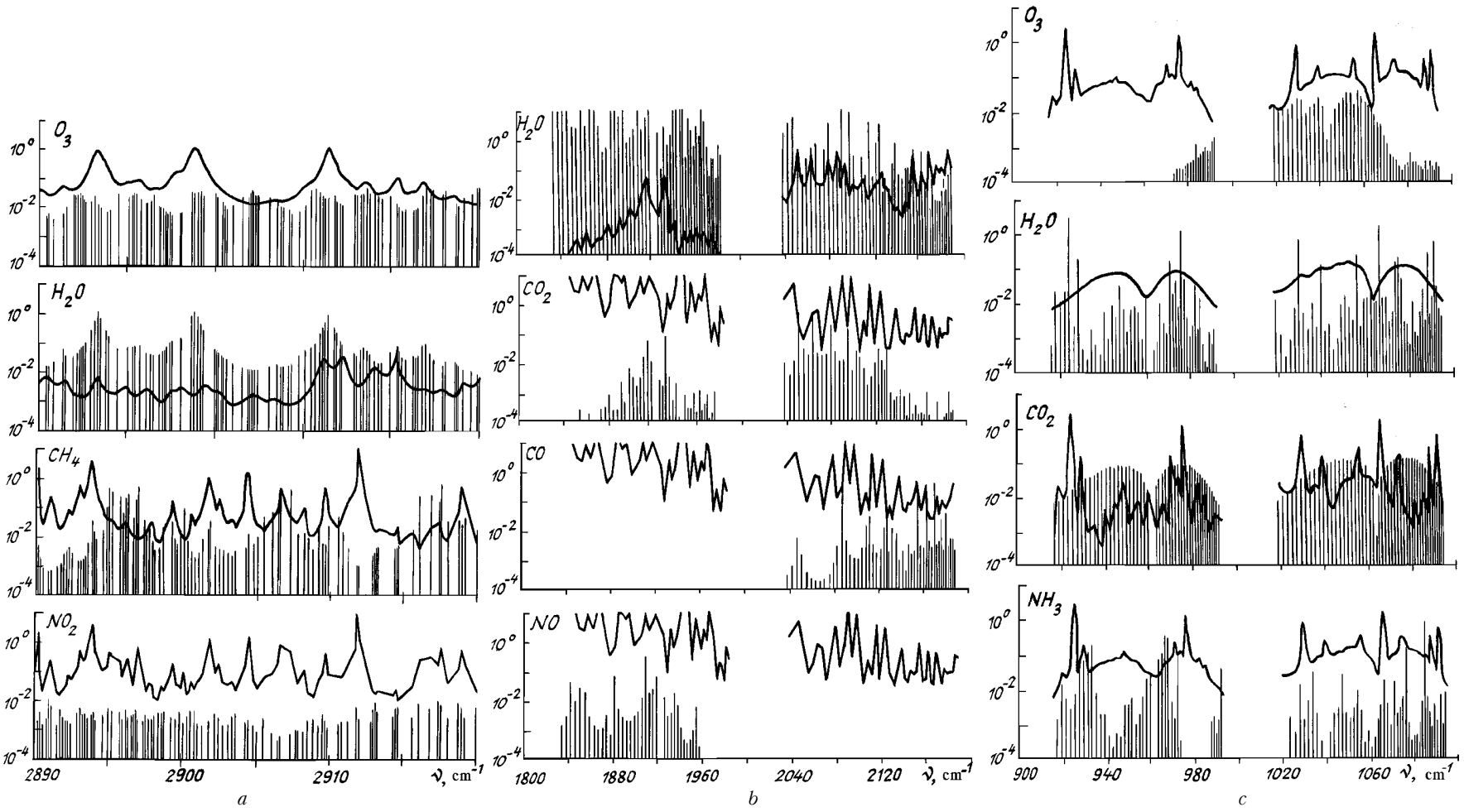

FIG. 2. The absorption coefficients (in km^{-1}*) of interfering (solid curves) and examined (vertical lines) gases. The atmospheric model is for the middle latitudes in summer. The conentrations of interfering gases are background:*

a) summed frequencies of the CO_2 *and* CO *lasers. The concentrations of the examined gases are* $\rho_{O_3} = 10^3 \cdot \rho^{bg}_{O_3}$; $\rho_{H_2O} = \rho^{bg}_{H_2O}$; $\rho_{CH_4} = \rho^{bg}_{HC_4}$; $\rho_{NO_2} = \rho^{bg}_{NO_2}$;

b) the second harmonics of a CO_2 *laser; the concentrations of the examined gase are:* $\rho_{H_2O} = \rho^{bg}_{H_2O}$; $\rho_{CO_2} = \rho^{bg}_{CO_2}$; $\rho_{CO} = \rho^{bg}_{CO}$; $\rho_{NO} = 10^3 \cdot \rho^{bg}_{NO}$; *and,*

c) fundamental frequencies of CO_2 *laser* $\rho_{O_3} = \rho^{bg}_{O_3}$; $\rho_{H_2O} = \rho^{bg}_{H_2O}$; $\rho_{CO_2} = \rho^{bg}_{CO_2}$; $\rho_{NH_3} = 200\ \rho^{bg}_{NH_3}$; *The contitual absorption by* H_2O *was ignored.*

TABLE II. Results of selection of the optimum line pairs for measuring.

Gas	Frequencies	AC ($cm^{-1}\cdot atm^{-1}$)	Background (β)	MDC (ppm) d_{fl} = 0.01–0.05	
				δ_{sys} = 0.01	δ_{sys} = 0.3
H_2O	10*P*(40)	$1.5\cdot10^{-3}$	0.61	140–340	1700–2000
	10*R*(20)	$6.6\cdot10^{-4}$	0.66	330–820	4100–4800
CO_2	2×9*P*(36)	$9.5\cdot10^{-3}$	1.00	30–85	410–500
	2×9*P*(20)	$4.0\cdot10^{-3}$	0.41	42–85	
NO	2×10*P*(24)	2.5	1.31	0.14–0.41	2.1–2.5
O_3	9*P*(8)	12.5	0.60	0.018–0.045	0.21–0.27
	9*P*(14)	12.0	0.66		
	9*P*(12)	11.5	0.64		
NH_3	9*R*(30)	78	0.58	0.003–0.007	0.03–0.035
NO_2	10–9*P*(19)+9*R*(34)	3.8	0.20	0.035–0.054	0.15–0.17
	10–9*P*(17)+9*R*(18)		0.13		
	10–9*P*(19)+9*R*(20)		0.13		
	11–10*P*(21)+9*R*(34)	2.0	0.12	0.05–0.08	0.24–0.27
	11–10*P*(21)+9*R*(32)	2.4	0.13		
C_2H_4	10*P*(14)	35	0.70	0.006–0.016	0.08–0.094
CH_4	11–10*P*(18)+9*R*(28)	3.1	0.11	0.044–0.52	0.15–0.18
	10–9*P*(21)+9*R*(24)	2.5	0.19	0.06–0.08	0.31–0.36
	10–9*P*(21)+9*R*(6)	2.0	0.16		
C_6H_6	9*P*(30)	1.7	0.62	0.12–0.29	1.47–1.72
	9*P*(28)	1.1	0.88	0.25–0.60	3.1–3.4
CO	2×9*R*(30)	24	0.13	0.006–0.007	0.022–0.026
	2×9*P*(24)	23	0.51	0.008–0.018	0.090–0.104

Thus, the results of the MDC modeling for the one–wave method also allow us to indicate the most effective wavelengths for the quantitative analysis of multicomponent gaseous mixtures under conditions of overlapping of the absorption bands (lines) of examined and interfering gases. However, the sufficiently accurate determination of the gas concentrations can be obtained in this case only from the inverse problem solution based on the data of multiwave sounding.

THE TRAL–4 LASER GAS ANALYZER

The TRAL–4 base gas analyzer of differential absorption is the laser meter of the horisontal transparency and the concentration of the minor atmospheric gas components integrated along the path. The TRAL–4 is the stationary gas analyzer intended for indoors. It is located on the third floor of the High–Altitude Sounding Station of the Institute of Atmospheric Optics. Its block diagram is shown in Fig. 3. The gas–analysis path, on which the specular retroreflectors *6* and *8* are stationary mounted, is located between the Station and the Rubin hotel. The path length is 0.5 km. However, when the mirror *6* is used, the path length is equal to 1 km, and when the mirrors *6*, *7*, and *8* are used it is equal to 2 km.

As can be seen from Fig. 3, the gas analyzer setup includes three lasers: a He–Ne laser at discrete wavelengths of 0.63, 1.15, and 3.39 μm, a cw CO laser discretely tunable in the region 5.25–6.42 μm, and a cw CO_2 laser discretely tunable in the region 9.2–10.86 μm. The collimator *4* and *5* amplifies the beam by a factor of 100. The receiving telescope consists of the mirror *9* with the 0.5–m diameter and the flat mirror *10*.

The panoramic spectrum analyzer (PSA) visualizing the radiation wavelength, where λ_{CO_2} is observed in the first– and λ_{CO} in the second orders, is used to control the wavelength. The movable mirror *2* reflectes the radiation of the He–Ne laser on the path (the alignment of optical system and the path tracing are made at a wavelength of 0.63 μm).

The spectrophone *S* is employed for local measurements of gas samples and for an additional wavelength control, for example, using ammonia. The pyrodetectors are used as the detectors R_{ref} and R_s when the fundamental harmonics are used, while the pyrodetectors are substituted by the photodiodes HgCdTe, when the second harmonic of CO_2 laser is used.

To lengthen the list of sounded gases (CO and others) the second harmonic generator (SHG), with possible changing of monocrystal ($ZnGeP_2$, $AgGaS_2$, and so on), is included into the gas analyzer.

The TRAL–4 has the powerful computer complex IBM/PC (with the 286 processor, the 1–Mbytes operative memory, and the 40–Mbytes vinchester) capable to process the sounding data in real time.

The signals from the spectrophone and from the reference and signal detectors R_{ref} and R_s are amplified by the 237 selective amplifiers *11* with the error $\pm (6 + 2U_{max}/U - 1)\%$, detected, and integrated. The maximum output direct voltage is 1V. The output voltage from the amplifier was digitized by the special analog–to–digital converter (12 digits, 16 channels, and sampling frequency 20 kHz on the channel) and entered into the computer interface. The computational results are stored on the hard or floppy disks and can be displayed on the screen or printed in the form of tables or the curves of temporal behavior. Two modulators are shown in Fig. 3: M_1 modulates all the three lasers and M2 modulates a cw CO_2 laser only when the generator of second harmonic is used.

For control of the tuning of CO and CO_2 lasers and automatic adjustment of the SHG crystal at the synhronism

angle the computer DVK–3 placed next to the gas analyzer is used. While working on the path the operator starts the program of tuning pressing the key (to control the correctness of the wavelength selection on the PSA), after tuning the laser from one line to another, for example, from λ_{on} to λ_{off}, the program of digitizing and processing is started.

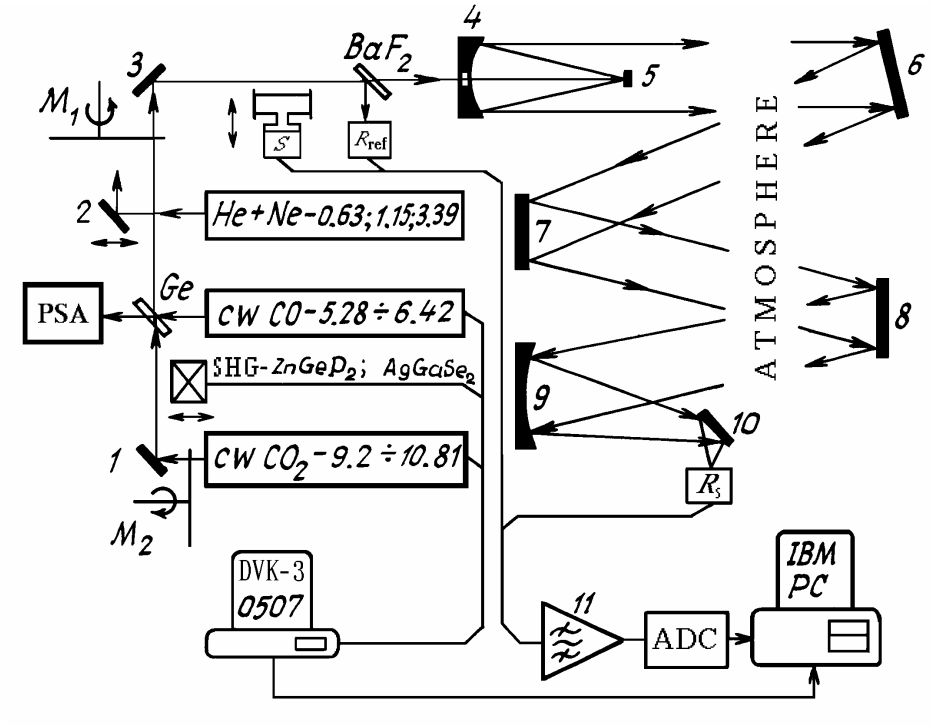

FIG. 3. A block diagram of the TRAL–4 laser gas analyzer.

MEASUREMENT RESULTS

The measurements with the TRAL–4 gas analyzer as part of the SATOR program were carried out in the industrial zone of Akademgorodok in Tomsk in June–July and October–November of 1991. The optical path was located at the altitude of 10–12 m between the High–Altitude Sounding Station and the Rubin hotel. For summer measurements the path length was 2 km and for the autumn ones it was 1 km. The concentrations of ozone O_3, water vapor H_2O, ammonia NH_3, ethylene C_2H_4, and carbon dioxide CO_2 were measured at different "on" and "off" line pairs of the CO_2–laser radiation. This pairs were

O_3	$-\ 9P28 - 9P24$;	$9P14 - 9P24$;
	$9P12 - 9P24$;	$9P08 - 9P24$;
H_2O	$-\ 10R20 - 10R16$;	$10P40 - 10P38$;
NH_3	$-\ 10R08 - 10R12$;	$10P32 - 10P30$;
	$9R30 - 9R28$;	$10R06 - 10R04$;
C_2H_4	$-\ 10P14 - 10P28$;	$10P14 - 10P22$;
	$10P14 - 10P18$;	$10P14 - 10P12$;
CO_2	$-\ 9P20 - 9P36$	$9P16 - 9P36$;

Figure 4*a* shows, using CO_2, C_2H_4, and O_3 as a point of reference, the satisfactory agreement of the calculated concentrations for the measurements at different line pairs. At the same time for water vapor and ammonia measured at different line pairs, the noticeable difference in the absolute values of measured concentrations can be seen (see Fig. 4*b*). This difference can be explained apparently by the influence of absorption of the CO_2 laser radiation by foreign gases.

The calculation of examined gas concentrations was performed in the experiment by two ways: without considering the foreign gas absorption at the selected line pairs (solid curves in Fig. 5) and taking into account the differential absorption $\Delta\beta$ of the other gases on and off absorption line of the examined gas (see Eqs. (9) and (10) and dash lines in Fig. 5).

However, as can be seen from Fig. 5 taking ozone as a point of reference, an account of the absorption coefficient under assumption of the background concentration of the foreign gases, has no marked effect on the temporal behavior of concentration, and its contribution to the absolute concentration values is not grater than 5 7%.

Thus, the situations shown in Fig. 4*b* are, probably associated with either the significant deviations of foreign gas concentrations from their background values or the presence of gases on the sounding path, which were ignored, but selectively absorb the sounding radiation.

For comparison the ozone concentrations measured simultaneously by two independent methods: with the laser gas analyzer (solid curves) and the 3.02*P* hemiluminescent ozone gas analyzer (dash curves) are shown in Fig. 6. They were obtained in the course of the All–Institute Ecological Experiment as part of the SATOR program. It can be seen that the measured concentrations can be very close in their absolute values, but in some cases they can be both larger and smaller. Moreover, the temporal behavior of the concentration can differ. The arising differences, probably, are explained, first, by the very nonuniform underlying surface of the laser gas–analysis path (trees, buildings, etc.) and, second, by the variability of the gas composition (influencing the ozone concentration) due to the pollution from the ventilation ejections from the industrial buildings located nearby. Thus,

the hemiluminescent gas analyzer installed on the first floor at the one end of the path and measuring at one point cannot reflect adequatively the situation on the entire optical path which is located at an altitude of 12 m. In addition, the ozone measurements by the hemiluminescent method are performed practically continuously and averaged over the large number of points while the laser gas–analysis data (due to the methodical reasons) are averaged over one–two points an hour. In addition, it should be noted that the ozone concentrations may undergo strong fluctuations (100–200%)

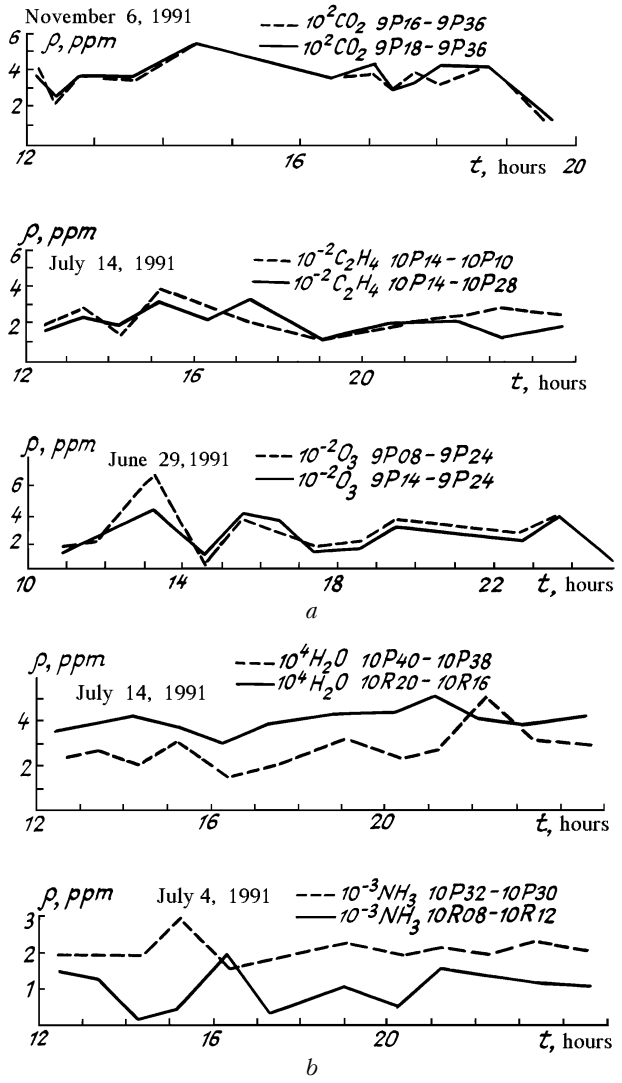

FIG. 4. Concentrations of the gaseous components measured at different "on" and "off" line pairs: a) carbon dioxide, ethylene, and ozone and b) the water vapor and ammonia.

for comparatively short time intervals due to the joint effect of different processes: photochemistry, wind and turbulent transport, presence of motor transport, and uncontrolled ejections of neighboring workshops. The phenomenon of fast variation of the ozone concentration was repeatedly recorded by the hemiluminescent method and was checked by the laser gas analyzer: as the measurement repetition frequency increased (up to 3–4 times an hour) the temporal behavior of ozone concentration becomes more variable (see, for example, the dash line in Fig. 7*c*). The range of ozone concentrations in individual cases varied from 5 to 80 ppb in summer. The mean concentrations were equal to 30–40 ppb. At night the ozone concentrations lowered noticeably, although in some cases, probably, owing to the peculiarities of the wind and turbulent transport from the possible anthropogenic sources, the night concentrations considerably exceeded the day level.

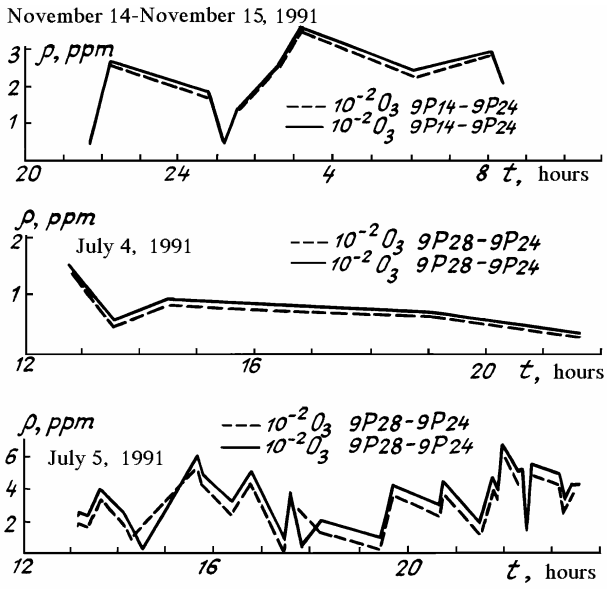

FIG. 5. The ozone concentrations calculated without (solid curves) and with (dash curves) an account of the absorption coefficients of interfering gases.

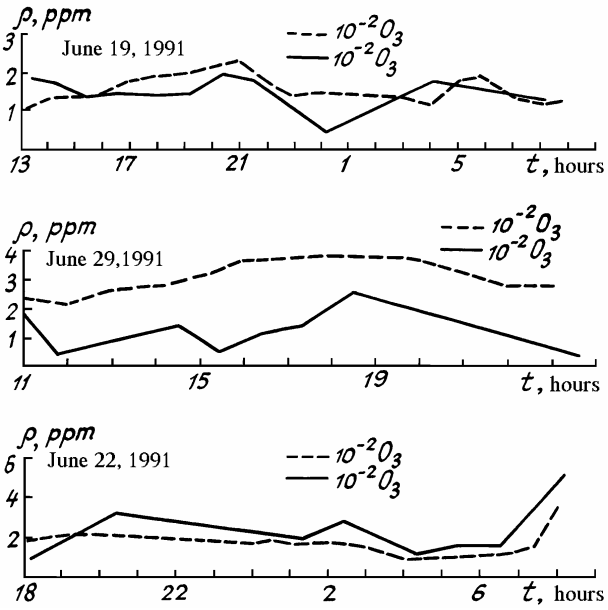

FIG. 6. The comparision of the ozone concentrations measured simultaneously with the laser (solid curves) and hemiluminescent (dash curves) gas analyzers.

The temporal behavior of the O_3 and CO_2 concentrations fixed on different days and for different atmospheric situations is shown in Fig. 7. It can be seen that in different situations the temporal behavior can be neutral as well as it can strongly fluctuate.

The limiting values of ozone, carbon dioxide, ammonia, water vapor, and ethylene concentrations recorded in June–July of 1991 are presented in Table III.

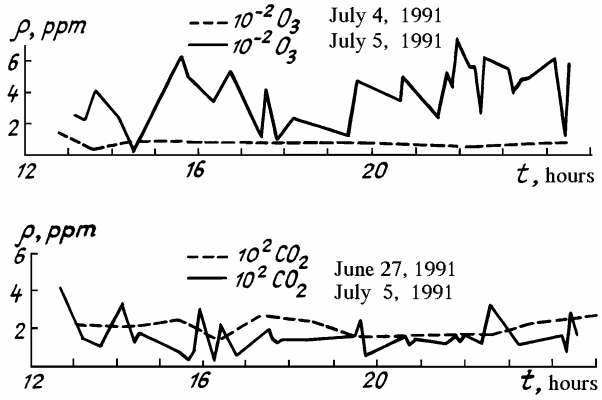

FIG. 7. Examples of different temporal behavior of concentration: practically neutral (dash curves) and strongly fluctuating (solid curves).

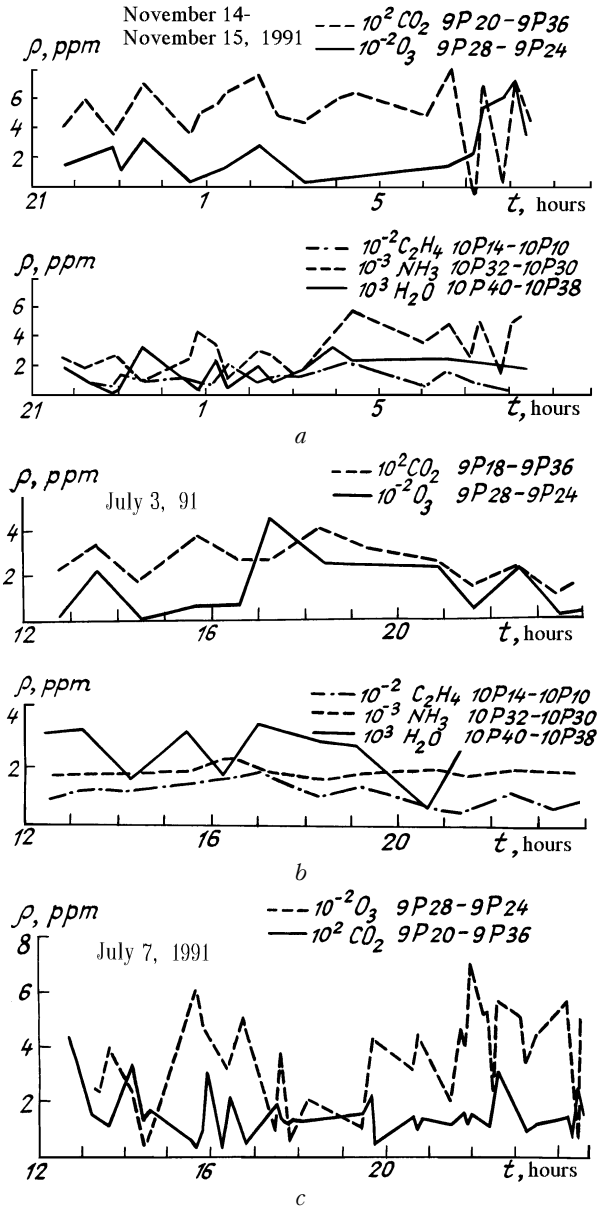

FIG. 8. Positive correlation between the variations of the ozone and carbon dioxide concentrations.

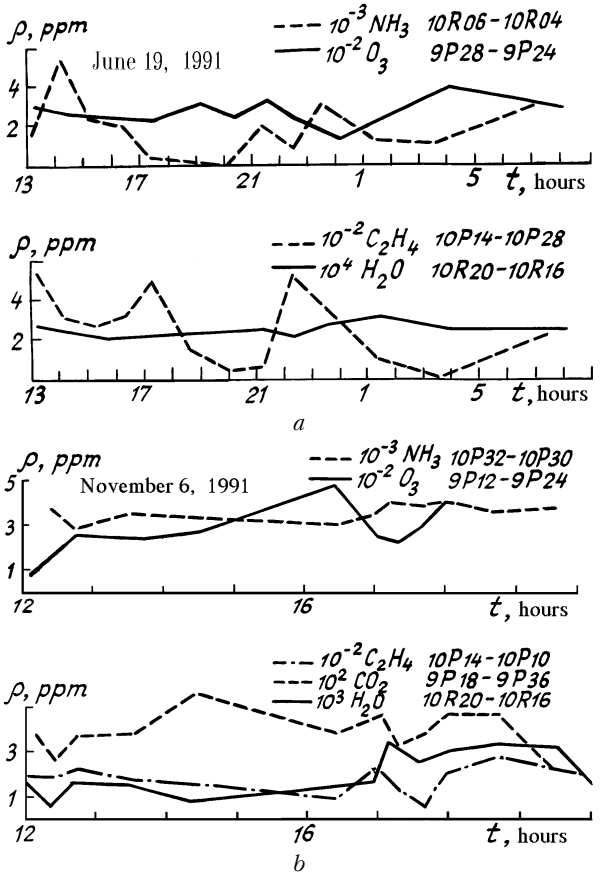

FIG. 9. Negative correlation between the variaitons of the ozone and ammonia concentration.

TABLE III.

Examined gas	Summer	Fall
Ozone	5–80 ppb	5–40 ppb
Water vapor	3000–40000 ppm	3000–30000 ppm
Ammonia	1–6 ppb	1–5 ppb
Carbon dioxide	100–700 ppm	100–600 ppm
Ethylene	20–40 ppb	10–40 ppb

In the course of accumulated data processing and the analysis of calculated concentrations of the examined gases, the positive correlation was found between ozone and carbon dioxide and the negative one between ozone and ammonia. The positive correlation between the variations of ozone and carbon dioxide concentrations (see Figs. 8*a*, *b*, and *c*) is probably, due to the sink of carbon oxide in the reaction with hydroxyl OH producing CO_2 (see Ref. 8).

$$CO + OH \rightarrow CO_2 + H\ . \qquad (23)$$

As can be seen, this reaction leads to the decrease of the OH concentration which is well known as one of the principal component decomposing ozone in the troposphere.

One of the possible reasons of negative correlation between the variations of the O_3 and NH_3 concentrations (see Fig. 9*a* and *b*) is the ammonia decomposition process and, in particular, its reaction with H_2O leading, in contrast to Eq. (23), to the hydroxyl OH formation[32]

$$NH_3 + H_2O \rightarrow NH_4 + OH \ . \quad (24)$$

which decomposes ozone.

The authors are sincerely grateful to the engineers O.V. Lagno and M.V. Grishaev for their assistance in preparing and carrying out the experiment as well as to the scientist G.N. Tolmachev who kindly provided the hemiluminiscent gas analyzer data and participated in the discussions of the obtained results.

REFERENCES

1. I.L. Karol', V.V. Pozanov, and Yu.M. Timofeev, *Gas Impurities in the Atmosphere* (Gidrometeoizdat, Leningrad, 1983), 192 pp.
2. A.S. Girgzhdis, in: *Monitoring of the Background Pollution of the Environment* (Gidrometeoizdat, Leningrad, 1986), No. 3, pp. 116–120.
3. R. Hasenclever, *Uber die Beschadingung der Vegetation durch Saure Gase* (Springer–Verlag, Berlin, 1978), 120 pp.
4. S. Mittler, in: *Toxicity of Ozone: I Acute Toxicity*, Ind. Med. Burg, 1956, pp. 301–306.
5. N.K. Frank and M.O. Amdur, Appl. Phys. **17**, 252–258 (1962).
6. W.W. Heck, O.C. Teylor, R. Adams, et al., Air Pollut. Control Assoc. **32**, No. 4, 353–361 (1982).
7. J.A. Logan, M.J. Pratter, S.C. Wolfsy, and McElroy, Trans. R. Soc., No. 290, 187–294 (1978).
8. *Atmosphere. Handbook* (Gidrometeoizdat, Leningrad, 1991) 510 pp.
9. J. Fishman, S. Solomon, P. Crutzen, Tellus **31**, 432–446 (1979).
10. F.Ya. Rovinskii and V.I. Egorov, *Ozone and Nitrogen and Sulfur Oxides in the Lower Atmosphere* (Gidrometeoizdat, Leningrad, 1985), 186 pp.
11. R.M. Measures, *Laser Remote Sensing* (John Wiley and Sons, New York, 1984).
12. V.R. Kozubovskii, Z.I. Perchi, and G.D. Romanenko, Kvantovaya Elektron. **18**, No. 5, 86–107 (1980).
13. W. Grat, *Laser Remote Sensing Techniques in Laser Monitoring of the Atmosphere* (Springer–Verlag, Berlin, 1987), 645 pp.
14. O.K. Kostko, V.S. Portasov, et al., *Application of Lasers for the Determination of Composition of the Atmosphere* (Gidrometeoizdat, Leningrad, 1983), 345 pp.
15. V.A. Beloborodov and A.I. Reshetnikov, *Devices for Remote Control of Environmental Gas Pollution* (Review), VNIIGMI–MCD, Obninsk, No. 3, 60 (1987).
16. L.S. Rothman, R.R. Gamache, A. Goldman, et al., Appl. Opt. **26**, No. 19, 4058–4097 (1987).
17. N. Husson et al., Ann. Geophys., No. 4, 185 (1986).
18. Yu.M. Andreev, P.P. Geiko, V.V. Zuev, et al., Opt. Atm. **1**, No. 2, 51–56 (1988).
19. Yu.M. Andreev, P.P. Geiko, A.I. Gribenyukov, et al., Opt. Atm. **1**, No. 3, 20–26 (1988).
20. V.V. Zuev and O.A. Romanovskii, Opt. Atm. **1**, No. 12, 29–32 (1988).
21. B.R. Levin, *Theoretical Foundations of Statistical Radio Engineering* (Nauka, Moscow, 1975), Vol. **2**, 392 pp.
22. M.Yu. Kataev, A.A. Mitsel', and S.R. Tarasova, Atm. Opt. **3**, No. 8, 763–772 (1990).
23. Yu.M. Andreev, V.V. Zuev, and O.A. Romanovskii, *"Automated system for searching after the optimum wavelengths for a laser gas analysis by the differential absorption method application,"* VINITI, No. 4058–B88, (1988) 32 pp.
24. E.D. Hinkley, ed. *Laser Monitoring of the Atmosphere* (Springer Verlag, New York, 1976).
25. A.A. Mitsel' and Yu.N. Ponomarev, *Optical Models of the Molecular Atmosphere* (Nauka, Novosibirsk, 1988), 128 pp.
26. G.M. Krekov and R.F. Rakhimov, *Optical Models of the Atmospheric Aerosol,* Tomsk Affiliate of the Siberian Branch of the Academy of Sciences of the USSR, Tomsk (1986).
27. V.N. Aref'ev, Kvantovaya Elektron. **12**, No. 3, 631–634 (1985).
28. G.P. Anderson, S.A. Clough, F.X. Kneizys, J.H. Chetwynd, and E.P. Shettle, AFGL–TR–86–0110, *Environmental Research Papers*, No. 954 (1986).
29. V.E. Zuev and V.S. Komarov, *Statistical Models of the Temperature and the Gaseous Atmospheric Components* (Gidrometeoizdat, Leningrad, 1986), 264 pp.
30. S.S. Penner, *Quantitative Molecular Spectroscopy and Gas Emittance* (Inostrannaya Literatura, Moscow, 1963), 415 pp.
31. L.I. Nesmelova, O.B. Rodimova, and S.D. Tvorogov, *Line Shape and Intermolecular Interaction* (Nauka, Novosibirsk, 1986), 215 pp.
32. *Chemistry. Handbook* [Russian translaiton] (Khimiya, Leningrad, 1975), 575 pp.